



Oxygen and magnesium mass-independent isotopic fractionation induced by chemical reactions in plasma

François Robert^{a,1}, Marc Chaussidon^b, Adriana Gonzalez-Cano^b, and Smail Mostefaoui^a

^aInstitut Origine et Evolution, Muséum National d'Histoire Naturelle, Sorbonne Université, IMPMC-UMR 7590 CNRS, 75005 Paris, France; and ^bUniversité de Paris, Institut de Physique du Globe de Paris, CNRS, F-75005 Paris, France

Edited by Mark Thiemens, Chemistry and Biochemistry, University of California San Diego, La Jolla, CA; received August 4, 2021; accepted November 8, 2021

Enrichment or depletion ranging from –40 to +100% in the major isotopes ¹⁶O and ²⁴Mg were observed experimentally in solids condensed from carbonaceous plasma composed of CO₂/MgCl₂/Pentanol or N₂O/Pentanol for O and MgCl₂/Pentanol for Mg. In NanoSims imaging, isotope effects appear as micrometer-size hotspots embedded in a carbonaceous matrix showing no isotope fractionation. For Mg, these hotspots are localized in carbonaceous grains, which show positive and negative isotopic effects so that the whole grain has a standard isotope composition. For O, no specific structure was observed at hotspot locations. These results suggest that MIF (mass-independent fractionation) effects can be induced by chemical reactions taking place in plasma. The close agreement between the slopes of the linear correlations observed between $\delta^{25}\text{Mg}$ versus $\delta^{26}\text{Mg}$ and between $\delta^{17}\text{O}$ versus $\delta^{18}\text{O}$ and the slopes calculated using the empirical MIF factor η discovered in ozone [M. H. Thiemens, J. E. Heidenreich, III. *Science* 219, 1073–1075; C. Janssen, J. Guenther, K. Mauersberger, D. Krankowsky. *Phys. Chem. Chem. Phys.* 3, 4718–4721] attests to the ubiquity of this process. Although the chemical reactants used in the present experiments cannot be directly transposed to the protosolar nebula, a similar MIF mechanism is proposed for oxygen isotopes: at high temperature, at the surface of grains, a mass-independent isotope exchange could have taken place between condensing oxides and oxygen atoms originated from the dissociation of CO or H₂O gas.

isotopes | MIF | plasma | cosmochemistry

Since their discovery in 1973 in the Calcium–Aluminum-rich inclusions (CAIs) of the carbonaceous chondrites (3), it has been shown that large enrichments and depletions in ¹⁶O were ubiquitous in the solar system, among meteorites, terrestrial planets, and the Sun (4–6) and a prominent feature of atmospheric chemistry (7–10). They were evidenced from the fact that, in a three-oxygen-isotope diagram, nearly all solar system samples have isotopic compositions (reported in ‰ variations as $\delta^{17}\text{O}$ versus $\delta^{18}\text{O}$ values, $\delta^m\text{O}_{\text{sample}} = [(R_{\text{sample}} / R_{\text{standard}}) - 1] \times 1,000$; with $R = {}^m\text{O}/{}^{16}\text{O}$ and $m = 17$ or 18) defining a linear correlation of slope close to 1 (hereafter referred to as 1:1 CL, the 1 to 1 correlation line), instead of a slope 0.52 for the “classical” mass-dependent isotopic fractionations (MDF) known to occur during physical and chemical processes (11). The question of the origin of the 1:1 CL is central to the formation of solids in the early solar system. It has been successively proposed to result from 1) the injection in the protosolar nebula (PSN) of pure ¹⁶O of supernovae origin (3), 2) a mass-independent fractionation (MIF) effect analogous to those observed experimentally during the synthesis of ozone (1, 7), and 3) a self-shielding effect on the solar (or nonsolar) ultraviolet light by CO (12–14). While the lack of presolar grains enriched in ¹⁶O makes the first proposal unlikely (15), the two other ones have gained some recent theoretical (14, 16) or experimental (17, 18) support. In the present paper, we address experimentally several issues raised by the ozone experiment to explore whether this 1:1 CL could be due to MIFs reactions having taken place in the PSN.

The formation of ozone results from a three-body reaction. However, at high temperature in a PSN dominated by H₂, the low concentration of elements heavier than H mean that three-body reactions cannot play an important role in the gas phase (16). In order to overcome this difficulty, the surfaces of growing grains were proposed as possible catalysts for the reactions leading to an MIF effect (16). Experimental evidence of this effect was reported for SiO/O₂/H₂ mixtures (17) but with variations of smaller magnitude than in solar system materials. The present paper is an additional test of this theoretical proposal.

Experimental

Because of the difficulties in carrying out controlled condensation experiments in hot plasmas, our approach was not intended to mimic the conditions of the PSN but to answer specific questions having key implications for cosmochemistry. Are oxygen MIFs linked to a precise class of chemical reactions? Are they restricted to gas phase reactions or, as suggested by ref. 18, can they take place during condensation of solids from a gas or be transferred from the gas to condensing solids? Can the conditions of the appearance of MIFs in the laboratory be reasonably extended to the conditions prevailing in the PSN? To this aim, we investigated reactions involving the isotopes of the two major elements constituting the telluric planets, O and Mg. The comparison between isotopic effects on O and Mg will bring important constraints because, at variance with O, all Mg isotopic fractionations in meteorites are considered to result from MDF processes such as evaporation, condensation, and diffusion (19–22).

Significance

Both the physical effect and the chemical conditions at the origin of the oxygen isotope variations in the solar system have been puzzling questions for 50 y. The data reported here bring the MIF effect (the mass-independent fractionation originally identified on ozone) back to the center of the debate. Similar to Ti isotopes, we observe that the MIF effect for O and Mg is triggered by redox reactions in plasmas. These observations reinforce the idea of a universal mechanism observable in photochemical reactions when molecular collisions involving indistinguishable isotopes yield a symmetrical complex stabilized as a chemical product.

Author contributions: F.R. designed research; F.R. performed research; A.G.-C. and S.M. contributed new reagents/analytic tools; F.R., M.C., A.G.-C., and S.M. analyzed data; and F.R. and M.C. wrote the paper.

The authors declare no competing interest.

This article is a PNAS Direct Submission.

This open access article is distributed under [Creative Commons Attribution-NonCommercial-NoDerivatives License 4.0 \(CC BY-NC-ND\)](https://creativecommons.org/licenses/by-nc-nd/4.0/).

¹To whom correspondence may be addressed. Email: francois.robert@mnhn.fr.

This article contains supporting information online at <http://www.pnas.org/lookup/suppl/doi:10.1073/pnas.2114221118/-DCSupplemental>.

Published December 23, 2021.

We have explored different reactions taking place in plasmas between gaseous species leading to the condensation of O- and Mg-bearing compounds. A summary of these experiments is shown in *SI Appendix, Table S1*. Here, we report only the results of experiments that have yielded MIF effects. The experimental protocol is comparable to that previously described for H or Ti (18, 23) and is detailed in *Material and Methods*.

In microwave plasma, the molecules are dissociated by electron impact producing highly reactive radicals. The high temperature of the gas enhances the rates of chemical or isotopic reactions. In addition, this type of plasma allows the condensation of enough material for isotopic analyses. The aim of these plasma experiments was to produce isotopic exchanges combined with chemical reactions. For oxygen isotopes, we studied the reactions between Pentanol and N₂O or between a solution of Pentanol-MgCl₂ and CO₂. The radical O atoms, produced by the dissociation of CO₂ or N₂O, react with their parent molecules and an isotopic exchange between O and CO₂ or between O and N₂O can take place. These isotopic exchanges are mediated by the transient formation of the activated complexes [CO₃]* or [N₂O₂]*. For magnesium isotopes, we studied the reaction between Pentanol and MgCl₂, for which the isotopic exchange can take place between Mg and MgCl₂ through the transient formation of the complex [Mg₂Cl₂]*. The purpose of the introduction of Pentanol along with the O and Mg gaseous carriers is to produce carbonaceous C_xH_y* radicals (23, 24) (dot designates radicals) that can react with the activated complexes before their dissociation as O+CO₂, O+N₂O, or Mg+MgCl₂. The reaction of the activated complex with a carbonaceous radical should lead to the retrieval of O and Mg from the gas by condensation via the polymerization of organic C_xH_y*-O or C_xH_y*-Mg macromolecules. An MIF effect is predicted in such a case, when an activated complex is involved in two chemical reactions (here dissociation or reaction with C_xH_y* radicals) at the same time because the rate of a chemical reaction involving a complex formed by identical isotopes is not the same than that of a complex formed by nonidentical (also referred to as indistinguishable) isotopes (25). Note that there is no scientific consensus on this interpretation (26).

Results

The Mg and O isotope compositions were measured using NanoSIMS at the Museum National d'Histoire Naturelle in Paris (*cf SI Appendix, Table S2* for instrumental setup). A selection of the data is reported in *SI Appendix, Table S3*. NanoSIMS analyses of the majority of the plasma deposited-carbonaceous material (PDCM) exhibit small isotopic variability, on the order of 10 to 30‰, likely due to analytical effects caused by surface sample roughness. In the following, PDCM will refer to this large fraction of condensed organic macromolecules that does not show any significant MIF effect. The measured isotopic variations are thus expressed in units using the average isotopic compositions (for O and Mg) of the PDCM as reference values. This procedure allows to minimize analytical matrix effects and to express the isotopic fractionation relative to the nonfractionated compounds produced from the same gas. Analyses of terrestrial samples with no MIF (San Carlos olivine and terrestrial kerogen) and of the PDCM show an external reproducibility (measured in a 10 μm² area) of ±~20‰ (2σ) for δ^{25,26}Mg and ±~30‰ (2σ) for δ^{17,18}O (*cf SI Appendix, Table S3.1 and Fig. S3.1 and SI Appendix, Table S3.3 and Fig. S3.3*).

The Mg and O isotopic results (Figs. 1 and 2 constructed from *SI Appendix, Table S3.2, S3.4, and S3.5*) show four major features: 1) Large MIFs distributing along a line of slope close to 1 are observed both for O and Mg in the experimental condensates. For Mg (Fig. 14) the observed slope (1.127 ± 0.034) is close to the calculated one (1.05 if mass-dependent effects are ignored; *cf SI Appendix, S4*) using the model developed for

MIF in ozone (18, 25). Similarly for O, the observed slopes (1.086 ± 0.048 for δ^{17,18}O < 0‰ and 1.066 ± 0.079 for δ^{17,18}O > 0‰, [ignoring data with δ¹⁸O > 250‰]) are close to the calculated one (1.00). Note that no free parameter is involved in the calculation of these theoretical MIF slopes. 2) MIFs appear specific to chemical reactions. In Fig. 2A, the negative δ¹⁷O - δ¹⁸O data correspond to the oxidation of Pentanol by N₂O (*SI Appendix, Fig. S5*), while the positive ones correspond to the oxidation of the Pentanol/MgCl₂ solution by CO₂. In the Pentanol/MgCl₂/CO₂ experiment, one area on the Si wafer shows variations distributed along a slope ≈0.5 but with an enormous range of variations in δ¹⁸O (from ~+700 to ~+1,500‰; Fig. 2A), impossible to explain by a “classical MDF.” 3) Oxygen isotopic variations along the 1:1 CL are not correlated to the ¹⁶O concentration (i.e., to the ion count rate; *cf SI Appendix, Table S3.5*), so that they cannot be explained by mixing between two components but requires instead variations in the magnitude of the MIF factor producing multiple end members. And 4), at the scale of 200 to 500 nm, MIFs are not systematically associated with elemental O hotspots (i.e., with an increase in the ionic emissivity of O compared to that from the amorphous PDCM, where no MIF effect is observed). Note that, in the case of the Pentanol/N₂O experiment, no hotspot in emissivity was observed at the location of negative MIF effects.

As reported in Fig. 1 in the case of the Pentanol/MgCl₂ experiments, isotopic Mg hotspots were clearly associated with the rim of carbonaceous grains (*cf ref. 27* for the formation of nanoparticles from plasma). As observed for Ti isotopes (18), the Mg MIF effect varies within the grains in such a way that the isotopic mass balance is achieved at the scale of the bulk grain. For experiments involving oxygen isotopes, the morphology of the grains carrying the MIF effect could not be determined, and it cannot be excluded that the MIF carriers are part of the molecular structure of the PDCM.

Discussion

Several theoretical origins of the MIF effect (i.e., the origin of the MIF factor noted η) have been proposed (26, 28–30). Here, we take for granted that the MIF effect appears when the activated complex responsible for the isotopic exchange is involved in a chemical reaction (6, 16, 25).

Reaction 1; cf. Materials and Methods

For the CO₂/MgCl₂/Pentanol experiment, the complex is likely [CO₃]* (31). Because 1) no oxygen MIF effect is observed in the Pentanol/CO₂ experiment (*cf SI Appendix, Table S1*) and because 2) at the location of oxygen MIF chlorine is observed by scanning electron microscopy as ~200-nm spots while Mg is absent, the MIF effect is attributed to the reaction of [CO₃]* with an organochlorine radical (C_xH_y-Cl)*. The complex [CO₃]* can either decompose and return to the gas (Channel 1 of the reaction 1) or be stabilized (Channel 2) as (C_xH_y-ClO). In this model, both Channels lead to an MIF effect with fractionation opposite in sign, but only the isotopic effect in the condensed phase can be preserved in the reaction products since isotopic re-equilibration will take place in the gas.

The lack of measurable MIF effects in the PDCM indicates that C_xH_y-O can also directly condense without reacting with the complex [CO₃]*. We thus now distinguish between two types of condensation: a complex-mediated condensation and a direct condensation (i.e., a two-body reaction). A similar scheme can be proposed to explain the Pentanol/N₂O experiment, where the complex would be [N₂O₂]*.

The present experimental observations can be tentatively extended to the origin of oxygen isotopic variations in the PSN. A possible scenario—alternative to the self-shielding ones (12–14)—can be proposed (Fig. 3A and B).

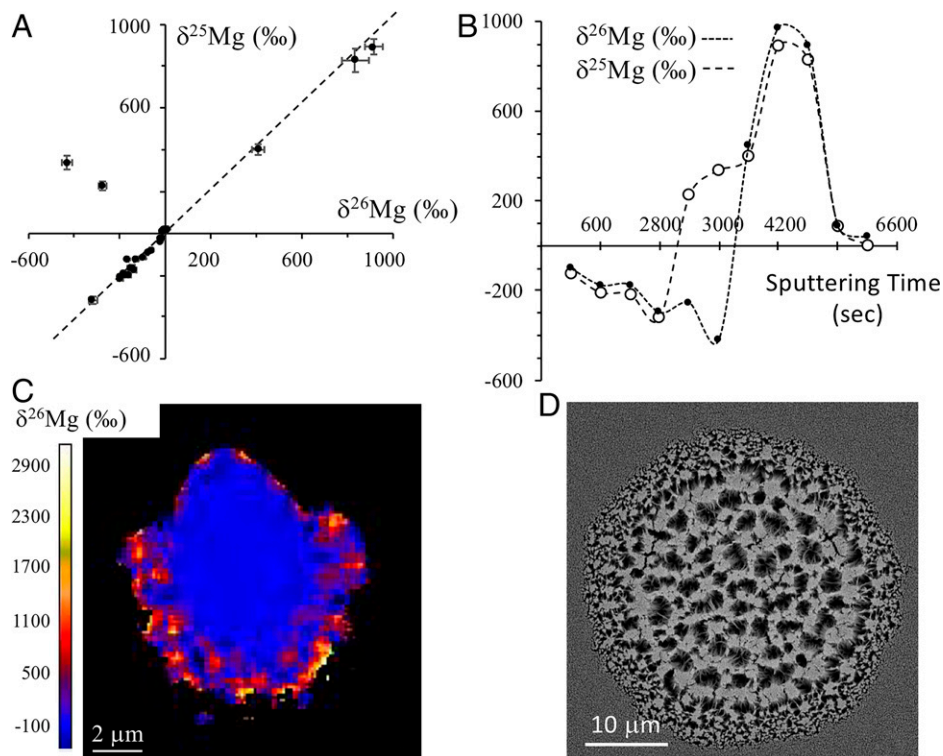


Fig. 1. (A) Magnesium isotopic compositions of Mg-bearing carbonaceous grains reported as $\delta^{25}\text{Mg}$ versus $\delta^{26}\text{Mg}$ variations relative to the PDCM ($0:0 \pm \approx 20\%$). Data were collected in four grains either as surface or volume variations (cf *SI Appendix, Table S3.2*). Error bars include statistical errors (ion counting statistic) and the reproducibility on the standard ($\pm 2\sigma$). The 1:1 dashed line is drawn for reference but does not stand for the best fit line to the data. (B) $\delta^{26}\text{Mg}$ and $\delta^{25}\text{Mg}$ variations of the rim of the 5- μm size grain shown in Fig. 1C are reported as a function of the analytical sputtering time expressed in seconds (data also reported in Fig. 1A). The total sputtering duration (6,600 s) indicates that the rim of the grain is ~ 200 nm thick. The PDCM ($\delta^{26}\text{Mg} \approx \delta^{25}\text{Mg} \approx 0\%$) embedding the grain reappears after complete sputtering. Note the two-outlier data (which are not analytical errors) observed during the flipping from negative to positive values (also obvious in Fig. 1A). Cf. sample *Robert-Juillet-2019_23.im* in *SI Appendix, Table S3.2*. (C) Ionic image of the distribution of $\delta^{26}\text{Mg}$ shown in Fig. 1B. This image is made by the summation of the three scans collected between 3,600 and 4,800 s (cf Fig. 1B). The core of the grain (in blue) has a homogeneous isotopic composition ($\delta^{26}\text{Mg} \approx \delta^{25}\text{Mg} \approx 0\%$), while the rim exhibits marked enrichments in ^{26}Mg (^{25}Mg not reported here) localized in spots that do not exceed 200 nm in size. The PDCM where the $\delta^{25}\text{Mg}$ and $\delta^{26}\text{Mg}$ cannot be defined because of the too-low counting rates on ^{25}Mg and ^{26}Mg appears in black. (D) Secondary Electron Microscopy image of another Mg-bearing carbonaceous grains (not analyzed for isotopic analyses) deposited on the silicon wafers. The structure suggests that the extreme isotopic variations observed in the grain shown in (C) are concentrated in the fine-grained rim.

Reaction 2 (cf. Materials and Methods). In this scenario, E is a chemical element ($E = \text{Si}, \text{Al}, \text{Mg}, \text{Ca}, \text{etc.}$) forming an oxide EO that condenses from the gas phase. O_{Ads} and EO_{Ads} correspond to species adsorbed at the surface of a solid (subscript Ads in Reaction 2) during its condensation, so that the formation rate of $[\text{EO-O}]_{\text{Ads}}^*$ is enhanced by many orders of magnitude relative to the rate in gas phase reaction. Note that contrary to the self-shielding model, the dissociation of $\text{H}_2\text{O}_{\text{Gas}}$ or CO_{Gas} does not produce MIF fractionated oxygen atoms (O_{Gas}). The oxygen isotope exchange takes place in $[\text{EO-O}]_{\text{Ads}}^*$ and produce the MIF effect during its decomposition. The Channel 1 corresponds to the stabilization of a fraction of the complex $[\text{EO-O}]_{\text{Ads}}^*$ in the solid (subscript Sol) by unknown reactions. The dashed arrows for the Channel 2 indicate that the other fraction of the complex $[\text{EO-O}]_{\text{Ads}}^*$ can be either incorporated in the solid (Channel 2a) as observed here for Mg and for Ti (32) isotopes or can spontaneously dissociate to the gas phase (Channel 2b). The O returned to the gas by this destabilization of a fraction of the complex, re-equilibrates isotopically with the major oxygen-bearing molecules of the PSN (H_2O and CO). The magnitude and the sign of MIF in the two fractions of the complex stabilized in the solid are expected to depend on the type of chemical reaction taking place, as observed in the present experiments with oxidation of pentanol by either N_2O or CO_2 producing either ^{16}O excess or ^{16}O depletion, respectively (Fig. 2). In other words, if

this mechanism occurs in the PSN, different oxides must have different MIF factors.

This catalytic property of grain surfaces for enhancing the rate of reaction between adsorbed species overcomes one of the major difficulties for having MIF effects in the PSN. Indeed, in the PSN, in a large excess of H_2 , the O atoms produced by the photodissociation of H_2O or CO (33) are likely to react with H_2 to form $\text{OH} + \text{H}$ much faster than being involved in a gaseous three-body reaction similar to that which leads to ozone (16). However, the chemical nature of the adsorbed activated complex taking part to condensation reactions in the PSN is, at this stage, impossible to predict. This is exemplified by the fact that no MIF is observed in meteorites for Mg, while large MIFs are produced in our experiments. This may indicate that the possible activated complexes involving two Mg atoms are unstable (such as $[\text{Mg}_2\text{O}]^*$) in the chemical conditions that prevailed during the condensation of Mg-rich silicates (forsterite could for instance form by direct condensation and not by a complex-mediated condensation).

Thus, assuming that the gas from which the first oxides and silicates condense in the PSN has the isotopic composition measured for the Solar wind ($\delta^{17}\text{O} \sim \delta^{18}\text{O} \sim -60\%$) (4, 5), only the grains condensed by a complex-mediated condensation would develop MIF effects with $\delta^{17}\text{O} \sim \delta^{18}\text{O}$ either > -60 (34) or $< -60\%$ (35, 36). All the other condensates, formed by direct

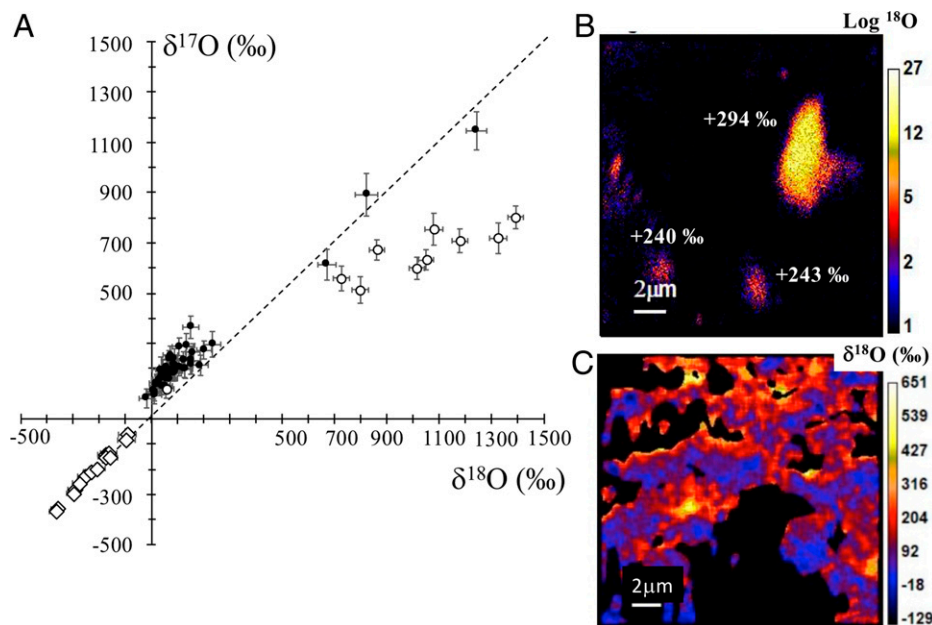


Fig. 2. (A) Oxygen isotopic compositions of grains embedded in the PDCM are reported as $\delta^{17}\text{O}$ versus $\delta^{18}\text{O}$. The variations are expressed relative to PDCM ($0\text{-}0\text{‰} \pm \approx 30\text{‰}$; 2σ). Error bars include statistical errors (ion counting statistic) and the reproducibility on the standard ($\pm 2\sigma$). Open diamonds stand for the oxidation of Pentanol by N_2O . Open and black dots stand for the oxidation of the $\text{MgCl}_2/\text{Pentanol}$ solution by CO_2 (open dots for grains concentrated in the same $100 \times 100\text{-}\mu\text{m}$ area and defining a slope ≈ 0.5). The 1:1 dashed line is drawn for reference, not for the best fit line. The correlation defined by the black dots does not intercept at $0\text{-}0\text{‰}$; this can be an analytical matrix effect or a MDF contribution to the MIF effect. (B) NanoSIMS ion image ($20 \times 20 \mu\text{m}$; sample *Robert-Juillet-2020_9* in *SI Appendix, Table S3.5*) showing four hotspots in oxygen intensities where MIF compositions were measured and reported in *SI Appendix, Fig. S6* (PDCM in black). The measured $\delta^{17}\text{O}$ are reported on the figure for three of the four hotspots. In order to increase the contrast of the image, the colors vary according to the logarithmic intensity of the ^{18}O count rate (Cps for counts/s). (C) NanoSIMS ion image ($20 \times 20 \mu\text{m}$; sample *Robert-Juillet-2020_18* in *SI Appendix, Table S3.5*) showing isotopic hotspots on Si wafer (in $\delta^{18}\text{O}$ (‰) units).

condensation, would have the oxygen isotopic composition of the PSN (Fig. 3B). Note however that due to mass balance effects, a gaseous reservoir previously fractionated by complex-mediated condensation could produce, by direct condensation, solids with MIF effects.

The simultaneous occurrence of these two types of condensation reactions, having different consequences as far as oxygen isotopes are concerned, may account for part of the large diversity of isotopic compositions observed in CAIs and chondrules from primitive meteorites (34). Note however that the large

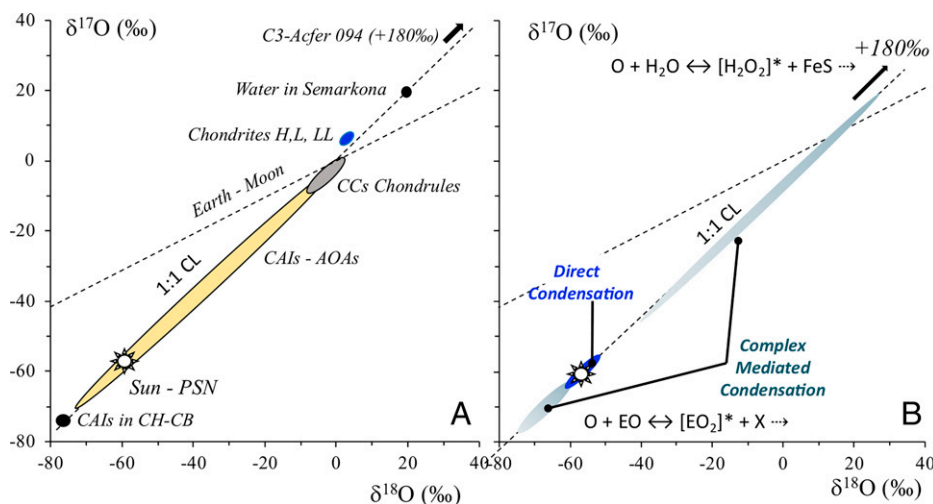


Fig. 3. (A) $\delta^{17}\text{O}$ versus $\delta^{18}\text{O}$ diagram for the solar system. Selection of observational constraints. The MDF line (slope 0.52) is shown for the Earth–Moon system (dashed line). Minerals from refractory inclusions (CAIs), ameboid olivine aggregates (AOAs), and chondrules in carbonaceous chondrites define the 1:1 CL. Sun: $\delta^{17,18}\text{O} \approx -60\text{‰}$ (5). Some rare CAIs, relict CAIs in chondrules, and chondrule from CH-CB chondrites are enriched in ^{16}O relative to the Sun (35, 36). Extreme ^{16}O depletion was observed in the C3-Acfer 094 meteorite (38). Most meteorites (Chondrites H, L, and LL), the Earth, Moon, and Mars have bulk $\delta^{17,18}\text{O}$ values around $0 \pm 10\text{‰}$. (B) Qualitative interpretation of (A). The PSN gas has the oxygen isotopic composition of the Sun: $\delta^{17,18}\text{O} \approx -60\text{‰}$. The position of the grains on the 1:1 line is, at first order, dictated by the chemical reaction responsible for the complex-mediated condensation of oxides and silicates (noted $[\text{EO}_2]^*$ with E designating Si, Mg, Al etc.). Oxides would exhibit either ^{16}O depletion or enrichment relative to the Sun. The extreme ^{16}O depletion observed in the C3-Acfer 094 meteorite could result from a reaction involving one of the $[\text{O-H}_x\text{O}]^*$ complexes resulting from the dissociation of H_2O (37). Condensation taking place without going through an activated complex (noted direct condensation) should yield grains having the oxygen isotopic composition of the ambient gas, which can be different from the Sun if this gas was previously fractionated by complex-mediated condensation.

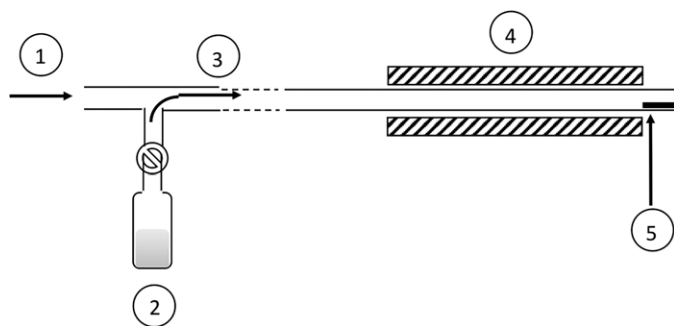
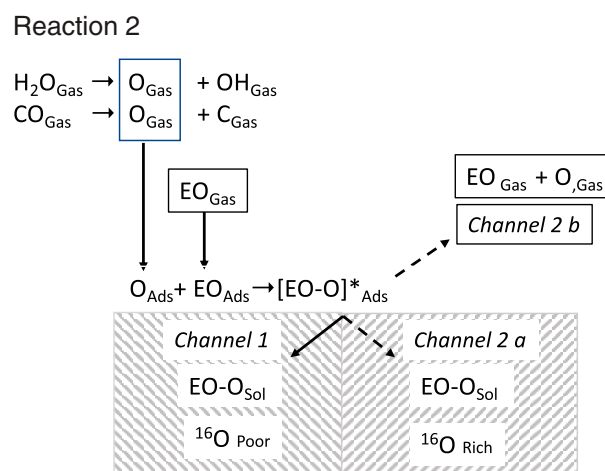
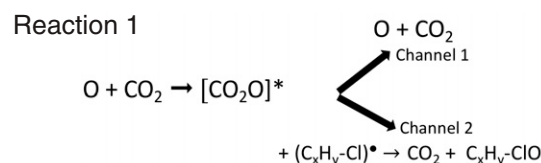


Fig. 4. (1) Gas vector (N_2 or N_2O or CO_2), (2) Reservoir of organic liquids (Pentanol or Pentanol- $MgCl_2$), (3) Leak of (2) in the gas vector, (4) Microwave cavity, and (5) Silicon Wafer. Organic deposits are present on the glass walls of region 4 and on the Wafer. Reaction 1: Possible reaction at the origin of the oxygen MIF effect observed in the $CO_2/MgCl_2$ /Pentanol plasma experiment. Reaction 2: Proposed chemical scheme at the origin of the mass-independent oxygen isotopic reaction observed in solar system materials.



$\delta^{17}O \approx \delta^{18}O$ variations observed in the present experiments (several hundreds of ‰) compared with the much smaller in $\delta^{17,18}O$ variations relative to the Sun observed in most solar system solids (50 to 70‰) implies that their oxygen isotopic composition contains only a small MIF contribution.

As postulated in the Reaction 2 and observed during the formation of SiO (17), complexes (37) resulting from the dissociation of H_2O could be responsible for the extreme ^{16}O depletion ($\delta^{17,18}O$ up to +180‰) observed (38) in some rare minerals whose synthesis involves the reaction between Fe (or FeS) and $H_2O^{(38)}$ (cf Fig. 3B).

Although the self-shielding model remains a viable possibility in the PSN to produce reservoirs variously depleted or enriched in ^{16}O (12, 13), the presently proposed MIF constitutes an additional potential source of ^{16}O enrichments and depletion. This scenario is testable in laboratory through dedicated experiments of high-temperature oxide condensation.

Materials and Methods

Experimental Protocol. All experiments (cf the schematic drawing in Fig. 4) were performed in a glass line, where the pressure reaches 10^{-4} Torr. A gas vector (N_2 for the Mg experiment and N_2O or CO_2 for the oxygen experiments) is injected into the line and passes through a cylinder glass tube ($\varnothing = 1$ cm, $l = 10$ cm), where the pressure is maintained at ≈ 1 Torr by dynamic pumping. Glass reservoirs containing organic liquids (Pentanol or $MgCl_2$ dissolved in Pentanol) were connected to the line by stopcocks. The vapor pressure of the liquids was injected in the gas vector by adjusting the leak of these stopcocks. The gas to organic pressure ratio was of the order of 1:1. The characteristic lifetime of the gas in the tube was 1/10 s. The plasma was produced in the center of the glass tube by a high frequency discharge at 2,450 MHz. In such conditions, the molecular temperature is estimated to be around 1,000 K. The plasma is not thermal (i.e., the temperature of the electrons is higher than that of the molecules).

Silicon wafers were deposited 5 cm downhill from the discharge. Carbonaceous matter was deposited on the glass walls around the discharge and on the silicon wafers. It was mechanically collected as a powder for isotopic analyses. The molecular organic structure of this carbonaceous matter is described elsewhere (39). Except for experiments involving N_2O , MIF effects were found

on the wafers. Except for Mg, no structural grain corresponding to the size and distribution of isotopic hotspots was identified by SEM.

We report in this paper only experiments where MIF effects were identified (other experiments are listed in *SI Appendix, Table S1*). It should be kept in mind that MIF-bearing grains are rare in the organic matter (named PDCM for plasma deposited carbonaceous matter for the organic matter with no significant MIF). So, the fact that no MIF region was observed in these samples is not definitive proof that they are absent.

Analytical Protocol. The Mg and O isotope compositions were measured using NanoSIMS at the Museum National d'Histoire Naturelle in Paris. The isotopic compositions of individual grains (\varnothing 0.5 to 2 μm) were analyzed by image analysis using the *I'Image* software package (L. Nittler, Carnegie Institution of Washington, Washington, DC). For NanoSIMS analyses, carbonaceous powder collected on the glass walls (region 4 in Fig. 4) were pressed on gold, gold coated, and mounted on 1-inch holders. Silicon wafers are gold coated without any further preparation. The instrumental parameters of the NanoSIMS are reported in *SI Appendix, Table S2*.

In order to have comparable topographic and matrix effects for the isotopic reference and for the samples, all data are reported using the PDCM as the reference value. In others terms, the isotopic fractionation is expressed relative to the carbonaceous deposits that do not show MIF effects in excess of $\approx \pm 2\sigma$ relative to their average value. When analyses were performed randomly, each area ($20 \times 20 \mu m$) was divided in 9 regions (i.e., ROI [Region of Interest] $\approx 6 \times 6 \mu m$; noted "Random Area" in *SI Appendix, Table S3.3 and S3.5*). Data reported in *SI Appendix, Table S3.2, S3.4, and S3.5* are used to construct the figures in the text. Two examples of the distribution of the Mg and O data recorded on the PDCM are shown in *SI Appendix, Fig. S3.1 and S3.3*.

Analyses on terrestrial kerogen powders give reproducibility of ± 37 and ± 23 on $\delta^{17}O$ (‰) and $\delta^{18}O$ (‰), respectively (2σ), similar to those measured for the PDCM. Under the same conditions, the reproducibility on the polished San Carlos olivine standard is $\approx \pm 8$ and $\approx \pm 5$ on $\delta^{17}O$ (‰) and $\delta^{18}O$ (‰), respectively. The poor reproducibility on the PDCM is caused by the topography of the organic powder pressed in gold, bearing in mind that the presence of non-detected MIF-bearing grains cannot be totally excluded.

For magnesium, a synthetic sample (Methylmagnesium chloride evaporated in the air) was used to verify the MDF relations between the electron multipliers. For oxygen, these relations are checked routinely for rock sample analyses.

Data Availability. All study data are included in the article and/or *SI Appendix*.

ACKNOWLEDGMENTS. This work was supported by grants from the National Center for Scientific Research MITI (ISOTOP 2020, COSMIFs) from ANR (ANR-20-CE49-0011-01). F.R. acknowledges support (Overheads) from European

Research Advanced Grant *PaleoNanoLife* (Principal Investigator: F.R.; 161764). We thank Florie Lopus for her availability and efficiency, without which the

realization of these experiments would not have been possible. Sylvain Pont's contribution was appreciated for SEM analyses.

1. M. H. Thiemens, J. E. Heidenreich, 3rd, The mass-independent fractionation of oxygen: A novel isotope effect and its possible cosmochemical implications. *Science* **219**, 1073–1075 (1983).
2. C. Janssen, J. Guenther, K. Mauersberger, D. Krankowsky, Kinetic origin of the ozone isotope effect: A critical analysis of enrichments and rate coefficients. *Phys. Chem. Chem. Phys.* **3**, 4718–4721 (2001).
3. R. N. Clayton, L. Grossman, T. K. Mayeda, A component of primitive nuclear composition in carbonaceous meteorites. *Science* **182**, 485–488 (1973).
4. K. Hashizume, M. Chaussidon, A non-terrestrial ^{16}O -rich isotopic composition for the protosolar nebula. *Nature* **434**, 619–621, (2005).
5. K. D. McKeegan *et al.*, The oxygen isotopic composition of the Sun inferred from captured solar wind. *Science* **332**, 1528–1532 (2011).
6. E. D. Young, K. Kuramoto, R. A. Marcus, H. Yurimoto, S. B. Jacobsen, Mass-independent oxygen isotope variation in the solar nebula. *Rev. Mineral. Geochem.* **68**, 187–218 (2008).
7. M. H. Thiemens, Introduction to chemistry and applications in nature of mass independent isotope effects special feature. *Proc. Natl. Acad. Sci. U.S.A.* **110**, 17631–17637 (2013).
8. M. H. Thiemens, M. Lin, Use of isotope effects to understand the present and past of the atmosphere and climate and track the origin of life. *Angew. Chem. Int. Ed. Engl.* **58**, 6826–6844 (2019).
9. M. C. Liang, F. W. Irion, J. D. Weibel, G. A. Blake, C. E. Miller, Y. L. Yung, Isotopic composition of stratospheric ozone. *J. Geophys. Res.* **111**, D 02302 (2006).
10. A. H. Laskar, S. Mahata, S. K. Bhattacharya, M.-C. Liang, Triple oxygen and clumped isotope compositions of CO_2 in the middle troposphere. *Earth Space Sci.* **6**, 1205–1219 (2019).
11. E. D. Young, A. Galy, H. Nagahara, Kinetic and equilibrium mass-dependent isotope fractionation laws in nature and their geochemical and cosmochemical significance. *Geochim. Cosmochim. Acta* **66**, 1095–1104 (2002).
12. H. Yurimoto, K. Kuramoto, Molecular cloud origin for the oxygen isotope heterogeneity in the solar system. *Science* **305**, 1763–1766 (2004).
13. J. R. Lyons, E. D. Young, CO self-shielding as the origin of oxygen isotope anomalies in the early solar nebula. *Nature* **435**, 317–320 (2005).
14. J. R. Lyons, An analytical formulation of isotope fractionation due to self-shielding. *Geochim. Cosmochim. Acta* **282**, 177–200 (2020).
15. L. R. Nittler, Presolar stardust in meteorites: Recent advances and scientific frontiers. *Earth Planet. Sci. Lett.* **209**, 259–273 (2003).
16. R. A. Marcus, Mass-independent isotope effect in the earliest processed solids in the solar system: A possible chemical mechanism. *J. Chem. Phys.* **121**, 8201–8211 (2004).
17. S. Chakraborty, P. Yanchulova, M. H. Thiemens, Mass-independent oxygen isotopic partitioning during gas-phase SiO_2 formation. *Science* **342**, 463–466 (2013).
18. F. Robert *et al.*, Mass-independent fractionation of titanium isotopes and its cosmochemical implications. *Nat. Astron.* **4**, 762–768 (2020).
19. R. N. Clayton, R. W. Hinton, A. M. Davis, Isotopic Variations in the Rock-Forming Elements in Meteorites. *Philos. Trans. R. Soc. Lond. A* **325**, 483–501 (1988).
20. G. J. MacPherson, A. M. Davis, E. Zinner, The distribution of aluminum-26 in the early Solar System - A reappraisal. *Meteoritics* **30**, 365–389 (1995).
21. A. M. Davis, A. Hashimoto, R. N. Clayton, T. K. Mayeda, Isotope mass fractionation during evaporation of Mg_2SiO_4 . *Nature* **347**, 655–658 (1990).
22. E. D. Young, A. Galy, The isotope geochemistry and cosmochemistry of magnesium. *Rev. Mineral. Geochem.* **55**, 197–230 (2004).
23. F. Robert *et al.*, Hydrogen isotope fractionation in methane plasma. *Proc. Natl. Acad. Sci. U.S.A.* **114**, 870–874 (2017).
24. M. Scapinello, E. Delikonstantis, G. D. Stefanidis, The panorama of plasma-assisted non-oxidative methane reforming. *Chem. Eng. Process.* **117**, 120–140 (2017).
25. P. Reinhardt, F. Robert, On the mass independent isotopic fractionation in ozone. *J. Chem. Phys.* **513**, 287–294 (2018).
26. A. Teplukhin, D. Babikov, Properties of Feshbach and “shape”-resonances in ozone and their role in recombination reactions and anomalous isotope effects. *Faraday Discuss.* **212**, 259–280 (2018).
27. A. B. Murphy, Formation of titanium nanoparticles from a titanium tetrachloride plasma. *J. Phys. Appl. Phys.* **37**, 2841–2847 (2004).
28. Y. Q. Gao, R. A. Marcus, On the theory of the strange and unconventional isotopic effects in ozone formation. *J. Chem. Phys.* **116**, 137 (2002).
29. R. Schinck, P. Fleurat-Lessard, The effect of zero-point energy differences on the isotope dependence of the formation of ozone: A classical trajectory study. *J. Chem. Phys.* **122**, 094317 (2005).
30. M. V. Ivanov, D. Babikov, On molecular origin of mass-independent fractionation of oxygen isotopes in the ozone forming recombination reaction. *Proc. Natl. Acad. Sci. U.S.A.* **110**, 17708–17713 (2013).
31. B. L. Grigorenko, L. Duarte, I. V. Polyakov, A. V. Nemukhin, Theoretical characterization of the photochemical reaction $\text{CO}_2 + \text{O}(^3\text{P}) \rightarrow \text{CO} + \text{O}_2$ related to experiments in solid krypton. *Chem. Phys. Lett.* **746**, 137303 (2020).
32. F. Robert, P. Reinhardt, R. Tartese, Mass-independent fractionation of titanium isotopes. *Chem. Phys.* **540**, 110970 (2021).
33. M. L. Ovcharov, V. M. Granchak, Photocatalytic activation of carbon monoxide on semiconductors and derived nanocomposites: Basic principles and mechanisms: A review. *Theor. Exp. Chem.* **55**, 3 (2019).
34. A. N. Krot, K. Nagashima, J. R. Lyons, J.-E. Lee, M. Bizzarro, Oxygen isotopic heterogeneity in the early Solar System inherited from the protosolar molecular cloud. *Sci. Adv.* **6**, 42 (2020).
35. S. Kobayashi, H. Imai, H. Yurimoto, New extreme ^{16}O -rich reservoir in the early solar system. *Geochim. J.* **37**, 663–669 (2003).
36. M. Gounelle, A. N. Krot, K. Nagashima, A. Kearsley, Extreme ^{16}O enrichment in calcium–aluminum-rich inclusions from the Isheyevo(ch/cb) chondrite. *Ap. J.* **698**, L12–L22 (2009).
37. S. Pehkonen *et al.*, Photochemical synthesis of H_2O_2 from the $\text{H}_2\text{O}\dots\text{O}(^3\text{P})$ van der Waals complex: Experimental observations in solid krypton and theoretical modeling. *J. Phys. Chem. A* **111**, 11444–11449 (2007).
38. N. Sakamoto *et al.*, Remnants of the early solar system water enriched in heavy oxygen isotopes. *Science* **317**, 231–233 (2007).
39. K. Biron, S. Derenne, F. Robert, J. N. Rouzaud, Toward experimental synthesis of the chondritic insoluble organic matter. *MAPS* **50**, 1408–1422 (2015).